Brain-like networks of nanowires and nanoparticles: a change of perspective

Ryan. K. Daniels,[1] Matthew D. Arnold,[2] Zachary E. Heywood,[3]
Joshua B. Mallinson,[1] Philip J. Bones,[3] and Simon A. Brown[1,*]

[1]*The MacDiarmid Institute for Advanced Materials and Nanotechnology, School of Physical and Chemical Sciences, Te Kura Matū, University of Canterbury, Private Bag 4800, Christchurch 8140, New Zealand*

[2]*School of Mathematical and Physical Sciences, University of Technology Sydney, PO Box 123 Broadway NSW 2007, Australia*

[3]*Electrical and Computer Engineering, University of Canterbury, Private Bag 4800, Christchurch 8140, New Zealand*

(Dated: July 24, 2023)

Abstract

The connectivity of self-assembled networks of nanowires and nanoparticles is believed to strongly influence their performance in brain-like (neuromorphic) computing applications. Here we present a new perspective on the connectivity of these networks in which their neuron-like active elements are viewed in the same way as the nodes in artificial and biological neuronal networks. We consider two-dimensional and quasi-three-dimensional networks of nanowires and percolating networks of nanoparticles and show that, from this new perspective, they all have similar small-world characteristics. Other characteristics which may impact the computational performance of the networks are also investigated, including their assortativity and the scale-free nature of the nanoparticle networks. Taken together these results allow comparison of key network characteristics for a variety of self-assembled nanoscale networks, and provide a basis for detailed investigations of computational performance.

I. INTRODUCTION

Self-assembled networks of nanowires [1–13] and nanoparticles [14–24] have recently emerged as important candidate systems for brain-like (or neuromorphic) information processing. The essence of the approach is to take advantage of these networks' intrinsic dynamical properties to implement brain-inspired approaches to computation, such as Reservoir Computing (RC) [25, 26]. Implementation of such approaches in hardware has the potential to overcome limitations in traditional integrated circuit technologies [27, 28], while decreasing power consumption and improving performance [29, 30].

It is well-established that the intrinsic architectures of networks impact their dynamics, and in particular it has been shown that networks with scale-free and small-world properties provide important computational benefits [31–33]. There have therefore been significant efforts [9, 12, 18] to understand the connectivity of both networks of nanowires and nanoparticles (illustrated in the left column of Figure 1). The basis of this approach is to construct connectivity maps in which the nanowires and nanoparticles are the nodes of the networks, and the connections between them are links (illustrated in Figure 1, middle column, and discussed in detail below). This is a natural approach, and is necessary for, for example,

* simon.brown@canterbury.ac.nz

calculations of the electrical properties of the networks (through Kirchhoff's laws). However, in these static node maps (SNMs), the nodes are *passive, linear* elements (i.e. wires or particles) which do not modify signals that are transmitted through the network. This is very different to the situation in the biological brain and in artificial neural networks (ANNs) where the nodes are *dynamic, non-linear* elements, i.e. the nodes represent neurons which interact via (linear) synaptic connections.

This distinction is important because it has recently emerged that the memristive connections in self-assembled nanoscale networks exhibit dynamical, neuron-like behavior [7, 11, 20, 34]. Hence, it is clear that a change of perspective is required in order to compare the network characteristics of self-assembled networks with those of neural networks: the neuron-like active elements of the networks (the memristive junctions) should be considered as the nodes, and the connections between them (provided by the wires or particles) should be the passive, linear links, just as in biological and artificial NNs. This perspective is essential to the design of physical computing systems based on self-organised networks which aim to emulate the structure and associated functionality of neural networks. Here we present a detailed analysis of both nanowire networks (NWNs) and percolating networks of nanoparticles (PNNs) from this new perspective. As the cornerstone of this change in approach, which is explained in detail below, we introduce the concept of *dynamic* node maps (DNMs) for these networks. We present a detailed characterization of their properties and show that despite significant differences in the SNMs for NWNs as compared to PNNs, the DNMs are surprisingly similar to each other. We show that, in fact, the DNMs of *all* investigated networks exhibit small-world properties, i.e. they are highly clustered and have small path lengths between nodes [35], and all DNMs are assortative.

II. NETWORK MODELS

Both NWNs and PNNs (Figure 1, left column) are created using simple deposition processes [1–24]. The building blocks (nanowires, particles) are deposited randomly on insulating substrates and electrodes are provided to allow input signals to be injected into the networks, and outputs to be read, as required for computation. There are however key differences. Nanowires are typically surrounded by an insulating shell, so that when they land on previously deposited wires a memristive tunnel gap (Figure 1, center panel of left column

– see discussion in next section) is created at each point of contact between wires [1–3, 5]. The wires form quasi-three-dimensional (Q3D) stacks [12], but since the wires are often assumed to form perfectly planar, two dimensional (2D) networks, we consider both Q3D and 2D cases here. Nanowire deposition is simulated by randomly choosing the placement and orientation of the wires within a square deposition area. Where two wires intersect, a connection (memristive junction) is formed and the connectivity is stored in an adjacency matrix. Wires in the 2D networks are considered to be 1D lines, and therefore lie in a 2D plane and are allowed to inter-penetrate. Wires in the Q3D networks are considered to be 3D cylinders which stack vertically. Deposition occurs sequentially, with previous wires affecting the position of a new wire in 3D space. The plane has dimensions 30 μm and the wires are 6 μm long, which means that the percolation threshold is at $N \sim 140$ wires. For more details, see [12].

Metallic nanoparticles, on the other hand, have no protective shell and coalesce when they land on each other, forming extended, well-connected *groups* (Figure 1, bottom left); the deposition is terminated at the percolation threshold (onset of conduction) [14–16, 21] ensuring that the groups of particles are separated from one another by memristive tunnel gaps. The nanoparticles are simulated as uniform disks deposited randomly within a square deposition area, and are allowed to overlap with each other. This overlapping simulates the coalescence between neighboring particles, leading to the formation of groups of well-connected particles. When the surface coverage is below a critical threshold, no single group spans the entire deposition area. The conduction of the network is therefore due to the tunnel currents that flow across small gaps between groups. The centroids of the groups are taken to be the nodes, and the connections between groups, defined as the minimum distance between neighboring group boundaries, are stored in an adjacency matrix (as with the nanowire networks). For more details, see [12, 18, 19, 36].

We emphasize that after deposition the overall structure of both the NWNs and PNNs is fixed, and the dynamical (memristive) behavior takes place only in the tunnel gaps, where atomic or nanoscale filaments are formed. This is in contrast to other types of device in which memristive behavior results from significant re-arrangements of nanoparticles [37].

Both NWNs and PNNs can be considered within the framework of percolation theory, but experimental considerations mean that the two types of network are constrained in different ways. NWNs can be fabricated with a range of wire densities *above* the percolation threshold

[10], and so it is important to investigate the properties of networks as a function of the number of wires deposited (N), at a fixed system size. In contrast, PNNs are always prepared *at* the percolation threshold, and scaling laws [38, 39] suggest that network properties will change as a function of system size (we consider square systems of size $W \times W$ particle diameters). We therefore investigate the connectivity of NWNs and PNNs as a function of these different natural variables (i.e. N and W respectively), before comparing results and drawing conclusions.

III. DYNAMICAL, NEURON-LIKE BEHAVIOR IN TUNNEL GAPS

The basic non-linear units facilitating computation in the networks are the tunnel gaps. The tunnel gaps that form between neighboring nanoparticle groups and between touching nanowires act as switching sites: upon application of an external voltage stimulus, atomic scale filaments can be formed (and subsequently broken) in the tunnel gaps [14], resulting in changes in the gap conductance and consequently in the network conductance (G). These tunnel gaps, regardless of the type of system, are memristive: their resistance responds non-linearly to changes in applied voltage and exhibits memory of previous stimuli [40].

The atomic scale behaviour is illustated in Figure 1 (center panel of left column): when a bias voltage is applied across the gap, it causes the migration of ions and, depending on the system, an atomic or nanoscale filament begins to form [41–43]. In the low bias regime, the conductance is low because the current flow across the gap is via quantum tunneling. As the filament grows (shrinks), the width of the tunneling barrier decreases (increases), causing a non-linear change in conductance for each junction. At higher bias, the filament can bridge the gap, causing a transition to a high conductance Ohmic state.

Importantly, the effect of the applied electric field/current is cumulative, i.e., both formation and destruction of the atomic scale filaments can be viewed as integrating the applied signals until filament formation/destruction ('firing'). These processes are therefore qualitatively similar to integration and fire mechanisms in biological neurons [44, 45]. A variety of neuron-like behaviours have been described in different networks and individual devices, relying on both atomic scale and nanoscale mechanisms: the literature includes several studies that demonstrate brain-like properties such as neural avalanching and that compare experiments with simulations [7, 19] as well as recent reviews [10]. Note however that since the

focus of the present work is on the characteristics of the *networks* of memristive elements, neither the type of memristor under consideration nor the way that they are modeled affect the analysis presented below. It should also be emphasised that we are focused here on basic network characteristics (in the absence of stimuli) because the architecture of the network affects its dynamical properties, and hence its possible computational applications [7, 17, 19, 46].

IV. A CHANGE OF PERSPECTIVE

Figure 1 demonstrates the construction of dynamic node maps for all three types of networks (2D NWNs (top row, red), Q3D NWNs (centre row, blue) and PNNs (bottom row, green)). The left column in Figure 1 shows the physical network structure; the top view of the 2D and 3D NWNs are the same, as they differ only in their connectivity. The center column captures the connectivity of the networks in the corresponding static node maps: each wire or group of particles is a node in the network (black circles) and the links between them (colored lines) represent memristive tunnel gaps that connect the nodes. The right column in Figure 1 shows the transformation to the DNM, in which each neuron-like tunnel gap is represented as a colored node and the black lines represent passive links between them. The DNM is constructed simply by determining which *links* are connected via *nodes* in the corresponding SNM. This process is similar to the construction of so-called line graphs in graph theory [47]. The resultant DNM visualizes the connectivity between the active elements ('neurons' [7, 20]) and captures the topology of the artificial neural network contained within the NWN or PNN.

In the following we compare the detailed properties of the DNMs and SNMs, for all three network types.

V. RESULTS AND DISCUSSION

A. Basic connectivity analysis

We start by considering the degree of each node in the network maps and the lengths L of the paths between nodes. The degree, k, of a node is the number of links that connect that node to other nodes. Figure 2 shows the degree distributions ($n(k)$, left), for $N = 200$, 400,

600 (for the NWNs) and $W = 50$, 100, 200 (for the PNNs). The data for SNMs (DNMs) is shown with dashed (solid) lines. The degree distributions for NWNs are approximately normal, both for the SNMs and DNMs, but the distributions are broader for the 2D case (note the different horizontal scales in these two panels) because the wires all lie in a 2D plane, and therefore intersect all other wires deposited before or after them. In both 2D and Q3D networks, the DNMs have much larger mean degrees ($\bar{k} = \frac{1}{N}\sum_i^N k_i$; see Appendix A and in particular Figure A1, left column), although this difference is more striking in the 2D networks. In contrast the degree distributions for the PNNs are power-laws [18], with a shallower slope for the DNMs (note the logarithmic scales). The essential origin of these changes is that when the transformation to the DNMs occurs, there are many more nodes and connections between nodes than in the original SNMs (see Appendix B for an illustrative example and detailed discussion).

The path length between nodes i and j, L_{ij}, is the shortest sequence of links that connects them [35]. Figure 2 (right column) shows the path length distributions $n(L)$ for all networks. While there are some differences in detail, such as the increase in the width of the distributions for the Q3D NWNs compared to the 2D NWNs (the path between any pair of wires/junctions can be a complex route through the 3D stack, and paths can be circuitous, especially for small N), in each case the path length distributions for the static and dynamic node maps are remarkably similar to one another. This is simply because the number of nodes and links are directly related to each other, i.e. as the number of nodes increases in the SNMs, so too does the number of links (compare centre and right columns in Figure A1).

B. Small-world nature of the networks

Small world networks are highly clustered and have small path lengths between nodes [35]. It has previously been demonstrated that various biological and physical networks are small-world including *c. elegans* neural networks and macaque monkey brain regions [48, 49], and 2D NWNs [12, 50].

Figure 3 shows a comparison of the mean path lengths $\bar{L}$ (left column), mean local clustering $\bar{C}$ (middle column) and small world propensity (right column) for the SNMs (dashed lines) and DNMs (solid lines). Again each row corresponds to a different network type:

2D NWNs (top row, red), the Q3D NWNs (middle row, blue) and the PNNs (bottom row, green). All displayed quantities are the mean values obtained from 10 network realizations, with uncertainties representing standard deviations. $\bar{L}$ (i.e. $\frac{1}{N(N-1)}\sum_{i\neq j}^{N} L_{ij}$) increases at a slower rate for the Q3D networks than for the 2D networks. This is because wires at the top of the stack in the Q3D networks cannot connect with wires at the bottom [12]. For all networks, $\bar{L}$ for the dynamic node maps are very similar to those for the static node maps, reflecting the similarities in the path length distributions shown in Figure 2.

The second column in Figure 3 shows $\bar{C}$ for the different networks. For any node i with degree k_i, the local clustering coefficient [35] is given by

$$C_i = \frac{1}{k_i(k_i-1)} \sum_{j,k} A_{ij}A_{ik}A_{jk}, \tag{1}$$

where A_{ij}, A_{ik}, A_{jk} are elements of the adjacency matrix. The mean local clustering coefficient is then $\bar{C} = \frac{1}{N}\sum_{i=1}^{N} C_i$. The SNMs for the 2D NWNs and the PNNs have a high degree of clustering whereas those for the Q3D NWNs have low clustering, similar to random networks. However, after the transformation is made to the DNMs, clustering increases for all network types. The most dramatic increase is for the Q3D NWNs where the increase in $\bar{C}$ causes a significant increase in the small world propensity ϕ (Figure 3, right column, middle row). ϕ quantifies the small-world nature of the networks by mapping them onto corresponding regular and random Watts-Strogatz networks with the same number of nodes and degree distribution [48]:

$$\phi = 1 - \sqrt{\frac{\Delta_C^2 + \Delta_L^2}{2}}, \tag{2}$$

where the deviation of network clustering from those of a regular lattice is

$$\Delta_C = \frac{C_{latt} - \bar{C}}{C_{latt} - C_{rand}} \tag{3}$$

and the deviation of network path lengths from those of a random network is

$$\Delta_L = \frac{L_{obs} - L_{rand}}{L_{latt} - C_{rand}}. \tag{4}$$

Values of $\phi > 0.6$ signify small-world properties [48], and so *the DNMs are small-world for all network types*. This is a dramatic change for the Q3D NWNs, as the SNMs are *not* small-world. Remarkably, there is no significant change in small world character for the other network types, despite significant changes in the maps shown in Figure 1, and in the degree distributions (Figure 2).

C. Discussion of other network characteristics

The results presented in the previous sections establish a clear basis for comparison of the different networks of interest, using multiple different metrics. Since the transformation of the SNMs to DNMs results in rather similar small world characteristics for all networks we now consider some additional network properties that have previously been shown to be biologically relevant and to impact on computational performance in neural networks.

We begin by considering the *global* clustering for each network (Figure 4 (left column)), since it is correlated with the assortativity [51, 52] that will be discussed next. The global clustering coefficient [53] C_{global} is the ratio of closed triplets to all triplets:

$$C_{global} = \frac{\text{closed triplets}}{\text{open} + \text{closed triplets}}, \tag{5}$$

where an open triplet is defined as three nodes connected by two links, and a closed triplet is defined as three nodes connected by three links. In most cases, the global clustering coefficients are similar to the local clustering coefficients. The exception is for the PNNs where the transformation from the SNM to the DNM causes a dramatic change: the global clustering coefficients for the SNMs (DNMs) are significantly lower (higher) than the local clustering coefficients shown in Figure 3. This is because the calculation of the global clustering places greater (lesser) weight on high (low) degree nodes compared to the local clustering.

Assortativity is a measure of the correlation between nodes based upon some property [54]. For example in social networks, a person is more likely to be connected to people of a similar age rather than to people with radically different ages. The degree assortativity [54] is the Pearson correlation coefficient of the degree between pairs of connected nodes, given by

$$r = \frac{\sum_{ij} ij\,(e_{ij} - a_i b_j)}{\sigma_a \sigma_b}, \tag{6}$$

where e_{ij} is the fraction of links that connect nodes of degree i to nodes of degree j, and in undirected networks is symmetric. a_i and b_j are the fraction of links that start and finish at nodes with degrees i and j respectively (note that for undirected graphs, $a_i = b_j$). σ_a and σ_b are the standard deviations of the distributions a and b. Values of r vary between -1 and 1.

Here we examine assortativity based on the degree of each node. High assortativity in-

dicates that high (low) degree nodes are often connected to other high (low) degree nodes, whereas negative assortativity (also called disassortativity) indicates that high degree nodes are often connected to low degree nodes. Many biological networks are disassortative, contrasting with social networks which have high assortativity. Figure 4 (right column) shows the assortativity for each network. The SNMs for the Q3D NWNs are disassortative, and the corresponding DNMs are assortative, and a similar but more modest change is observed for the 2D NWNs (SNMs are assortative, and DNMs are highly assortative). This increase in assortativity is driven by the increase in global clustering since there is a clear correlation between high assortativity and networks with a transitive bias [51, 52] – when the global clustering is high (low), the assortativity is also high (low).

The change in assortativity for the PNNs is more dramatic. The SNMs for PNNs have the lowest (most negative) values of the assortativity among all networks considered here, whereas the corresponding DNMs are the most assortative. The wheel-and-spoke type pattern observed in the SNM (Figure 1, center panel of bottom row) is a common feature of disassortative networks with power-law degree distributions such as in *c. elegans* neural and protein connectivity maps [52, 55]. The high degree nodes act as hubs that connect mainly to smaller nodes with low-degree. This connectivity is destroyed in the transformation to the DNMs as the global clustering and therefore the assortativity increases dramatically, i.e. many tunnel gaps (nodes in the DNMs) have high k (see Figure 3) and are connected to other high k tunnel gaps via conducting groups of nanoparticles.

Assortativity has been shown to significantly impact computational performance [56], and it can influence the order of phase transitions and lead to explosive synchronization in oscillator networks [57]. Furthermore, it has been shown that robustness to noise is greatly enhanced in assortative neural networks, especially if it is the hub neurons that store the information, while disassortative networks are less resilient [58, 59]. This is highly relevant to the present work, because the dynamic node map perspective establishes the neuron-like memristive connections as the network node, and, at least for the PNNs, the effect of transforming the SNM to the DNM is dramatic. The present results are promising but it must be acknowledged that in each case the existing literature [56–59] focuses on specific types of neural or oscillator networks, and so it remains to be demonstrated whether the computational performance of the NWNs and PNNs will indeed be impacted by the particular network properties (scale-free, small world, local and global clustering, and assortativity)

studied here.

VI. CONCLUSION

In conclusion, we have presented a new perspective on the connectivity of nanowire and nanoparticle networks which leads to clear differences in topological properties (in comparison to previously published analyses), such as higher mean degrees and higher local clustering coefficients for all network types considered. We emphasize that while small-world properties of PNNs and NWNs have been identified previously [12, 50], neither the need to consider dynamic node maps, nor the properties of the DNMs have been considered previously. The key structural differences that underpin the differences in properties of the PNNs and NWNs are i) that in PNNs the nanoparticles overlap with each other to form groups of well-connected particles that are separated by tunnel gaps that have a range of sizes [19, 51], whereas nanowires are usually coated with materials that form relatively uniform memristive gaps between the wires [4]; and ii) the nanoparticles are deposited to the percolation threshold (so that the networks are poised at the threshold for conduction) whereas the NWNs are usually well above the percolation threshold.

The change of perspective presented here means that the neuron-like active elements in self-assembled nanoscale networks are viewed as equivalent to the nodes in artificial and biological neuronal networks. This change of perspective is required in order to allow direct comparison of properties of the networks (degree distributions, small world characteristics, assortativity) but we emphasise that the electrical characteristics of the NWNs and PNNs are unaffected: the application of Kirchhoff's laws requires the network to be considered from the point of view of the original static node maps. When considered as DNMs, 2D NWNs, Q3D NWNs and PNNs all have small world characteristics and high assortativity, suggesting that the performance of neuromorphic devices based on these networks might be similar. The main differences in the DNMs are that PNNs additionally have a scale-free network architecture similar to that of the biological brain [18]. This scale-free architecture, which is maintained in the transformation from SNMs to DNMs, is important for computational performance [46].

ACKNOWLEDGMENTS

The authors gratefully acknowledge financial support from the MacDiarmid Institute for Advanced Materials and Nanotechnology and the Marsden Fund, NZ.

[1] A. Z. Stieg, A. V. Avizienis, H. O. Sillin, C. Martin-Olmos, M. Aono, and J. K. Gimzewski, Emergent Criticality in Complex Turing B-Type Atomic Switch Networks, Advanced Materials **24**, 286 (2012).

[2] H. G. Manning, F. Niosi, C. G. da Rocha, A. T. Bellew, C. O'Callaghan, S. Biswas, P. F. Flowers, B. J. Wiley, J. D. Holmes, M. S. Ferreira, *et al.*, Emergence of winner-takes-all connectivity paths in random nanowire networks, Nature Communications **9**, 3219 (2018).

[3] H. Tanaka, M. Akai-Kasaya, A. TermehYousefi, L. Hong, L. Fu, H. Tamukoh, D. Tanaka, T. Asai, and T. Ogawa, A molecular neuromorphic network device consisting of single-walled carbon nanotubes complexed with polyoxometalate, Nature Communications **9**, 2693 (2018).

[4] A. Diaz-Alvarez, R. Higuchi, P. Sanz-Leon, I. Marcus, Y. Shingaya, A. Z. Stieg, J. K. Gimzewski, Z. Kuncic, and T. Nakayama, Emergent dynamics of neuromorphic nanowire networks, Scientific Reports **9**, 14920 (2019).

[5] G. Milano, G. Pedretti, M. Fretto, L. Boarino, F. Benfenati, D. Ielmini, I. Valov, and C. Ricciardi, Brain-inspired structural plasticity through reweighting and rewiring in multi-terminal self-organizing memristive nanowire networks, Advanced Intelligent Systems **2**, 2000096 (2020).

[6] Q. Li, A. Diaz-Alvarez, D. Tang, R. Higuchi, Y. Shingaya, and T. Nakayama, Sleep-dependent memory consolidation in a neuromorphic nanowire network, ACS Applied Materials & Interfaces **12**, 50573 (2020).

[7] J. Hochstetter, R. Zhu, A. Loeffler, A. Diaz-Alvarez, T. Nakayama, and Z. Kuncic, Avalanches and edge-of-chaos learning in neuromorphic nanowire networks, Nature Communications **12**, 4008 (2021).

[8] C. S. Dunham, S. Lilak, J. Hochstetter, A. Loeffler, R. Zhu, C. Chase, A. Z. Stieg, Z. Kuncic, and J. K. Gimzewski, Nanoscale neuromorphic networks and criticality: a perspective, Journal of Physics: Complexity **2**, 042001 (2021).

[9] A. Loeffler, R. Zhu, J. Hochstetter, A. Diaz-Alvarez, T. Nakayama, J. M. Shine, and Z. Kuncic, Modularity and multitasking in neuro-memristive reservoir networks, Neuromorphic Computing and Engineering **1**, 014003 (2021).

[10] Z. Kuncic and T. Nakayama, Neuromorphic nanowire networks: principles, progress and future

prospects for neuro-inspired information processing, Advances in Physics: X **6**, 1894234 (2021).

[11] G. Milano, G. Pedretti, K. Montano, S. Ricci, S. Hashemkhani, L. Boarino, D. Ielmini, and C. Ricciardi, In materia reservoir computing with a fully memristive architecture based on self-organizing nanowire networks, Nature Materials **21**, 195 (2021).

[12] R. K. Daniels and S. A. Brown, Nanowire networks: how does small-world character evolve with dimensionality?, Nanoscale Horizons **6**, 482 (2021).

[13] R. K. Daniels, J. B. Mallinson, Z. E. Heywood, P. J. Bones, M. D. Arnold, and S. A. Brown, Reservoir computing with 3d nanowire networks, Neural Networks **154**, 122 (2022).

[14] A. Sattar, S. Fostner, and S. A. Brown, Quantized Conductance and Switching in Percolating Nanoparticle Films, Physical Review Letters **111**, 136808 (2013).

[15] S. K. Bose, J. B. Mallinson, R. M. Gazoni, and S. A. Brown, Stable self-assembled atomic-switch networks for neuromorphic applications, IEEE Transactions on Electron Devices **64**, 5194 (2017).

[16] S. K. Bose, S. Shirai, J. B. Mallinson, and S. A. Brown, Synaptic dynamics in complex self-assembled nanoparticle networks, Faraday Discussions **213**, 471 (2019).

[17] J. B. Mallinson, S. Shirai, S. K. Acharya, S. K. Bose, E. Galli, and S. A. Brown, Avalanches and criticality in self-organized nanoscale networks, Science Advances **5**, eaaw8438 (2019).

[18] S. Shirai, S. K. Acharya, S. K. Bose, J. B. Mallinson, E. Galli, M. D. Pike, M. D. Arnold, and S. A. Brown, Long-Range Temporal Correlations in Scale-Free Neuromorphic Networks, Network Neuroscience **4**, 432 (2020).

[19] M. Pike, S. K. Bose, J. B. Mallinson, S. Acharya, S. Shirai, E. Galli, S. Weddell, P. Bones, A. M, and S. A. Brown, Atomic scale dynamics drive brain-like avalanches in percolating nanostructured networks, Nano Letters **20**, 3935 (2020).

[20] S. Acharya, E. Galli, J. B. Mallinson, S. K. Bose, F. Wagner, Z. Heywood, P. Bones, A. M, and S. A. Brown, Stochastic spiking behaviour in neuromorphic devices enables true random number generation, ACS Applied Materials and Interfaces **13**, 52861 (2021).

[21] C. Minnai, A. Bellacicca, S. A. Brown, and P. Milani, Facile fabrication of complex networks of memristive devices, Scientific Reports **7**, 7955 (2017).

[22] M. Mirigliano, F. Borghi, A. Podestà, A. Antidormi, L. Colombo, and P. Milani, Non-ohmic behavior and resistive switching of Au cluster-assembled films beyond the percolation threshold, Nanoscale Advances **1**, 3119 (2019).

[23] M. Mirigliano, D. Decastri, A. Pullia, D. Dellasega, A. Casu, A. Falqui, and P. Milani, Complex electrical spiking activity in resistive switching nanostructured Au two-terminal devices, Nanotechnology **31**, 234001 (2020).

[24] N. Carstens, B. Adejube, T. Strunskus, F. Faupel, S. Brown, and A. Vahl, Brain-like critical dynamics and long-range temporal correlations in percolating networks of silver nanoparticles and functionality preservation after integration of insulating matrix, Nanoscale Advances **4**, 3149 (2022).

[25] M. Lukoševičius and H. Jaeger, Reservoir computing approaches to recurrent neural network training, Computer Science Review **3**, 127 (2009).

[26] H. Jaeger, *Tutorial on training recurrent neural networks, covering BPPT, RTRL, EKF and the echo state network" approach*, Vol. 5 (GMD-Forschungszentrum Informationstechnik Bonn, 2002).

[27] M. M. Waldrop, The chips are down for Moore's law, Nature **530**, 144 (2016).

[28] I. L. Markov, Limits on fundamental limits to computation, Nature **512**, 147 (2014).

[29] G. Tanaka, T. Yamane, J. B. Héroux, R. Nakane, N. Kanazawa, S. Takeda, H. Numata, D. Nakano, and A. Hirose, Recent advances in physical reservoir computing: A review, Neural Networks **115**, 100 (2019).

[30] K. Nakajima, Physical reservoir computing—an introductory perspective, Japanese Journal of Applied Physics **59**, 060501 (2020).

[31] Z. Deng and Y. Zhang, Collective Behavior of a Small-World Recurrent Neural System With Scale-Free Distribution, IEEE Transactions on Neural Networks **18**, 1364 (2007).

[32] T. Nishikawa, A. E. Motter, Y.-C. Lai, and F. C. Hoppensteadt, Heterogeneity in oscillator networks: Are smaller worlds easier to synchronize?, Physical Review Letters **91**, 014101 (2003).

[33] Y. Kawai, J. Park, and M. Asada, A small-world topology enhances the echo state property and signal propagation in reservoir computing, Neural Networks **112**, 15 (2019).

[34] S. K. Bose, J. B. Mallinson, E. Galli, S. Acharya, C. Minnai, P. Bones, and S. A. Brown, Neuromorphic behaviour in discontinuous metal films, Nanoscale Horizons **7**, 437 (2021).

[35] D. J. Watts and S. H. Strogatz, Collective dynamics of 'small-world' networks, Nature **393**, 440 (1998).

[36] S. Fostner, R. Brown, J. Carr, and S. A. Brown, Continuum percolation with tunneling,

Physical Review B **89**, 075402 (2014).

[37] Y. Yang, B. Chen, and W. D. Lu, Memristive Physically Evolving Networks Enabling the Emulation of Heterosynaptic Plasticity, Advanced Materials **27**, 7720 (2015).

[38] D. Stauffer and A. Aharony, *Introduction to percolation theory* (CRC press, 2018).

[39] J. Schmelzer, S. A. Brown, A. Wurl, M. Hyslop, and R. J. Blaikie, Finite-Size Effects in the Conductivity of Cluster Assembled Nanostructures, Physical Review Letters **88**, 226802 (2002).

[40] D. B. Strukov, G. S. Snider, D. R. Stewart, and R. S. Williams, The missing memristor found, Nature **453**, 80 (2008).

[41] K. Krishnan, T. Tsuruoka, C. Mannequin, and M. Aono, Mechanism for conducting filament growth in self-assembled polymer thin films for redox-based atomic switches, Advanced Materials **28**, 640 (2016).

[42] H. Yang, Z. Wang, X. Guo, H. Su, K. Sun, D. Yang, W. Xiao, Q. Wang, and D. He, Controlled growth of fine multifilaments in polymer-based memristive devices via the conduction control, ACS Applied Materials & Interfaces **12**, 34370 (2020).

[43] W. Wang, M. Wang, E. Ambrosi, A. Bricalli, M. Laudato, Z. Sun, X. Chen, and D. Ielmini, Surface diffusion-limited lifetime of silver and copper nanofilaments in resistive switching devices, Nature Communications **10**, 81 (2019).

[44] A. N. Burkitt, A Review of the Integrate-and-fire Neuron Model: I. Homogeneous Synaptic Input, Biological Cybernetics **95**, 1 (2006).

[45] W. Gerstner, W. M. Kistler, R. Naud, and L. Paninski, *Neuronal Dynamics* (Cambridge University Press, Cambridge, 2014).

[46] J. B. Mallinson, Z. Heywood, R. K. Daniels, M. D. Arnold, P. J. Bones, and S. A. Brown, Reservoir Computing using Networks of Memristors: Effects of topology and heterogeneity, Nanoscale **15**, 9663 (2023).

[47] F. Harary, *Graph Theory* (Addison-Wesley Publishing Co., Boca Raton, 1969).

[48] S. F. Muldoon, E. W. Bridgeford, and D. S. Bassett, Small-world propensity and weighted brain networks, Scientific Reports **6**, 22057 (2016).

[49] D. S. Bassett and E. T. Bullmore, Small-world brain networks revisited, The Neuroscientist **23**, 499 (2017).

[50] A. Loeffler, R. Zhu, J. Hochstetter, M. Li, K. Fu, A. Diaz-Alvarez, T. Nakayama, J. M.

Shine, and Z. Kuncic, Topological properties of neuromorphic nanowire networks, Frontiers in Neuroscience **14**, 184 (2020).

[51] D. V. Foster, J. G. Foster, P. Grassberger, and M. Paczuski, Clustering drives assortativity and community structure in ensembles of networks, Physical Review E **84**, 066117 (2011).

[52] P. Holme and J. Zhao, Exploring the assortativity-clustering space of a network's degree sequence, Physical Review E **75**, 046111 (2007).

[53] S. Wasserman, K. Faust, *et al.*, *Social network analysis: Methods and applications* (Cambridge university press, Cambridge, 1994).

[54] M. E. Newman, Assortative mixing in networks, Physical Review Letters **89**, 208701 (2002).

[55] B. Bentley, R. Branicky, C. L. Barnes, Y. L. Chew, E. Yemini, E. T. Bullmore, P. E. Vértes, and W. R. Schafer, The multilayer connectome of caenorhabditis elegans, PLoS Computational Biology **12**, e1005283 (2016).

[56] C. Blasche, S. Means, and C. R. Laing, Degree assortativity in networks of spiking neurons, Journal of Computational Dynamics **7**, 401 (2020).

[57] M. Roy, S. Poria, and C. Hens, Assortativity-induced explosive synchronization in a complex neuronal network, Physical Review E **103**, 062307 (2021).

[58] M. Rubinov and O. Sporns, Complex network measures of brain connectivity: Uses and interpretations, Journal of Computational Dynamics **52**, 1059 (2010).

[59] S. de Franciscis, S. Johnson, and J. Torres, Enhancing neural-network performance via assortativity, Physical Review E **83**, 036114 (2011).

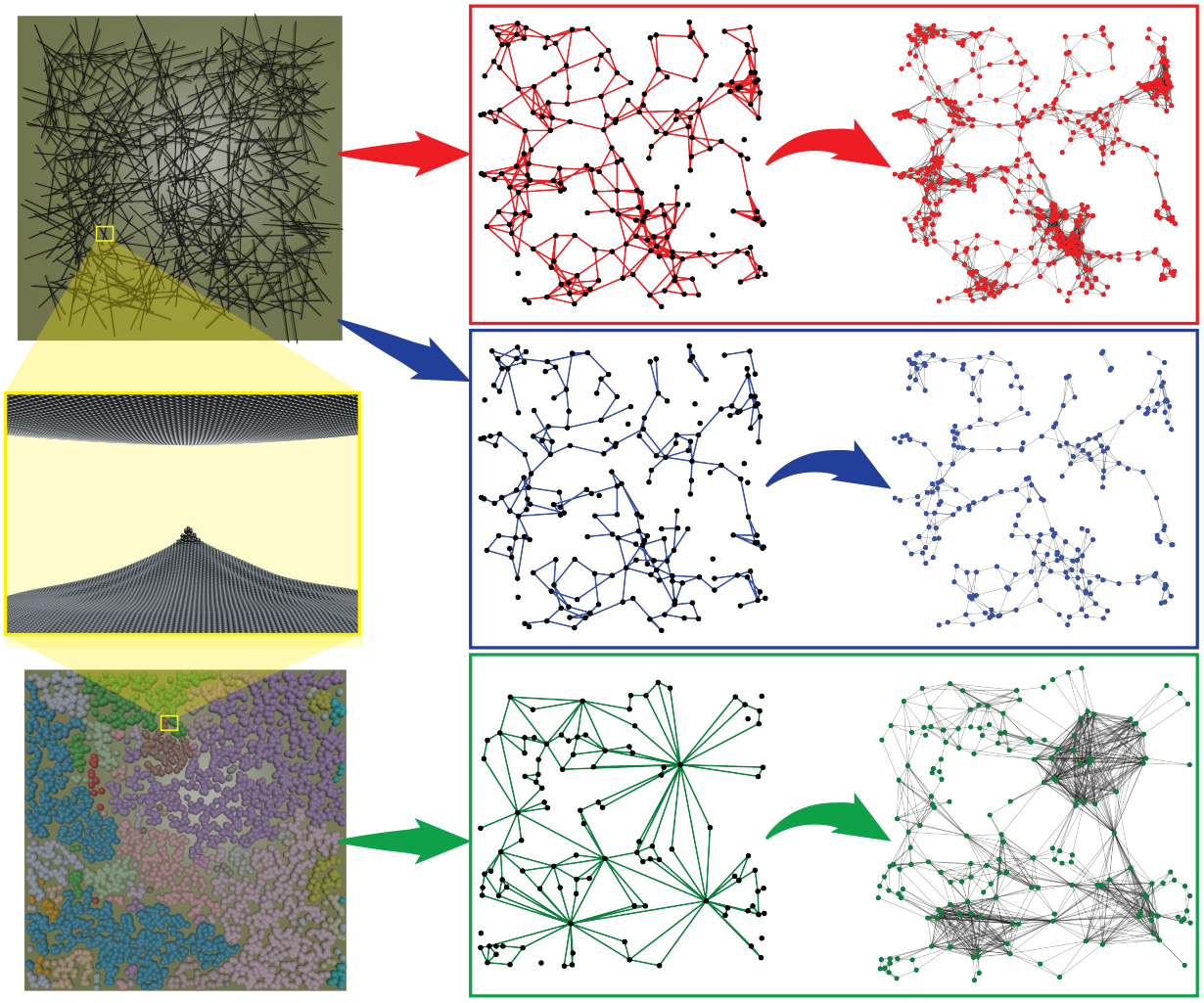

FIG. 1. Process for construction of dynamic node maps. The left column shows examples of a NWN (top) and a PNN (bottom), and the electric field driven formation of a 'hillock' of atoms in the tunnel gaps between the wires or nanoparticles (center). These hillocks are precursors to the formation of filaments that bridge the gaps and exhibit memristive properties – see main text. The middle column shows static node maps in which the wires and groups of nanoparticles are the nodes in the network. For the NWNs (2D (top row) and Q3D (middle row)), the nodes are the midpoints of the nanowires, and the links represent the memristive junctions formed between the wires. There are fewer connections in the 3D case because of stacking effects [12]. In the PNN (bottom), nanoparticles coalesce to form groups (each colored differently in the bottom left panel). The nodes are then the group centroids, and the links are gaps formed between groups (these are also the memristive junctions). The right column shows the dynamic node maps, in which the memristive junctions are the nodes of the networks and the links represent connections via wires/groups.

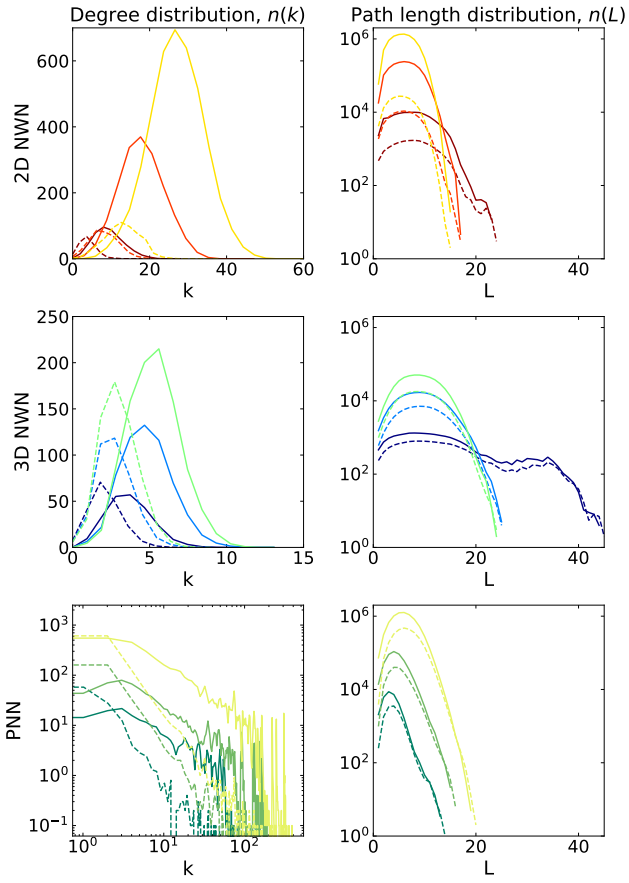

FIG. 2. Key characteristics of the networks. Left column: degree distributions $n(k)$; right column: path length distributions $n(L)$. 2D NWNs (top row, red), Q3D NWNs (middle row, blue) and PNNs (bottom row, green). SNMs: dashed lines; DNMs: solid lines. For the NWNs data is shown for $N = 200$, 400, and 600 wires and for the PNNs $W = 50$, 100, 200; the progression from dark to light colors indicates increasing N, W.

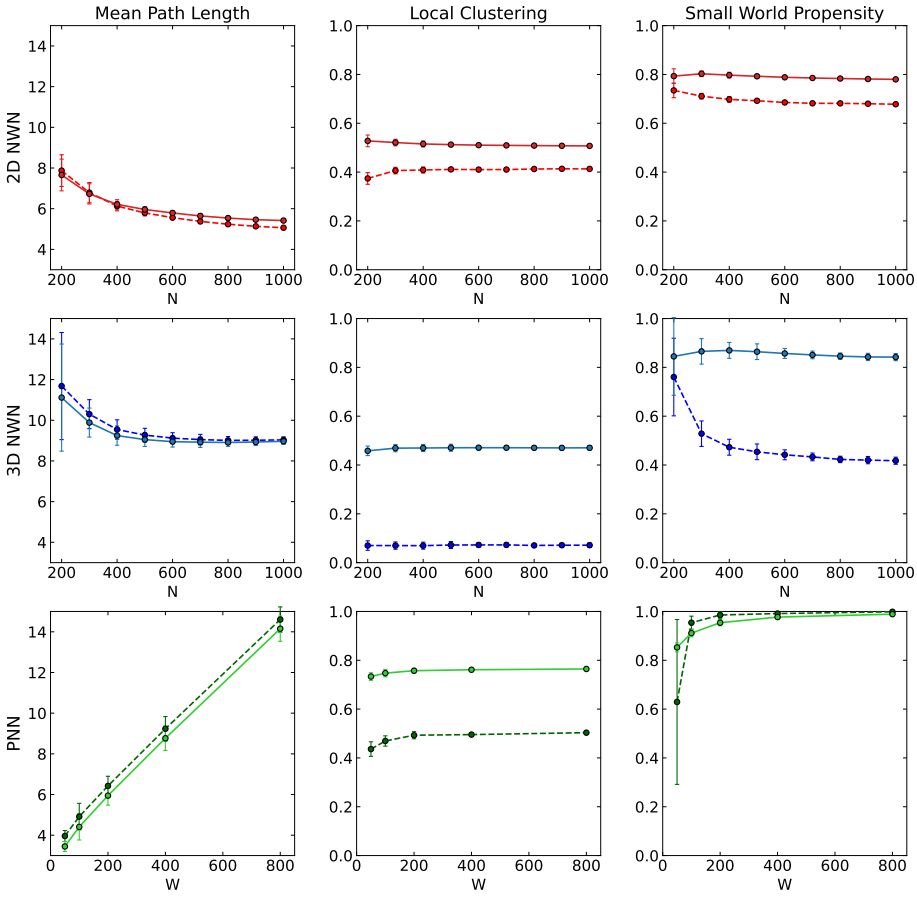

FIG. 3. Small-world nature of the networks. Dependence of mean path length (left), mean local clustering coefficient (middle), and small-world propensity (right) on the number of nanowires (N, for the NWNs) or the system size (W, for the PNNs). 2D NWNs (top row, red), Q3D NWNs (middle row, blue) and PNNs (bottom row, green). SNMs: dashed lines; DNMs: solid lines.

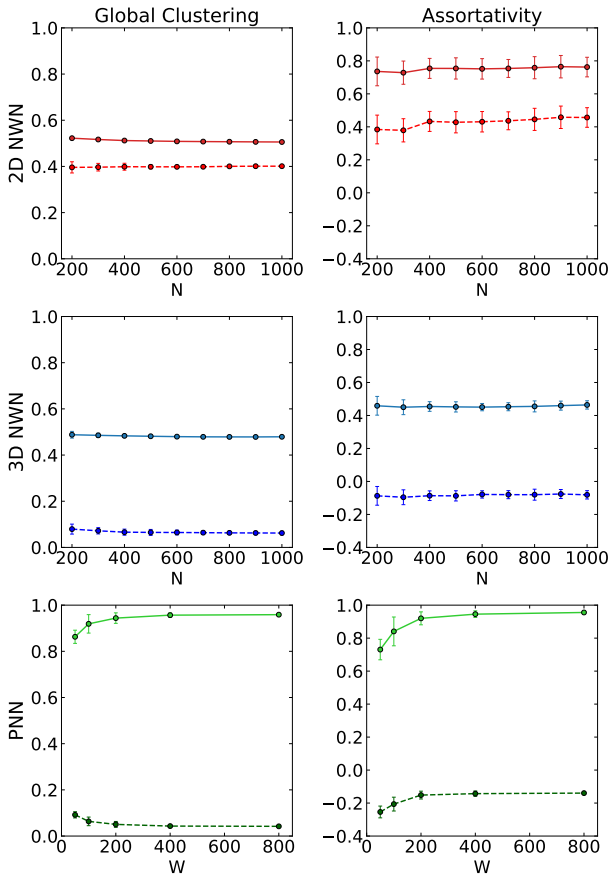

FIG. 4. Assortativity for the various networks. Dependence of the global clustering (left column) and assortativity (right column) on the number of nanowires (N, for the NWNs) or the system size (W, for the PNNs). 2D NWNs (top row, red), Q3D NWNs (middle row, blue) and PNNs (bottom row, green). SNMs: dashed lines; DNMs: solid lines.

APPENDIX A: MEAN DEGREE, NUMBER OF NODES AND NUMBER OF LINKS

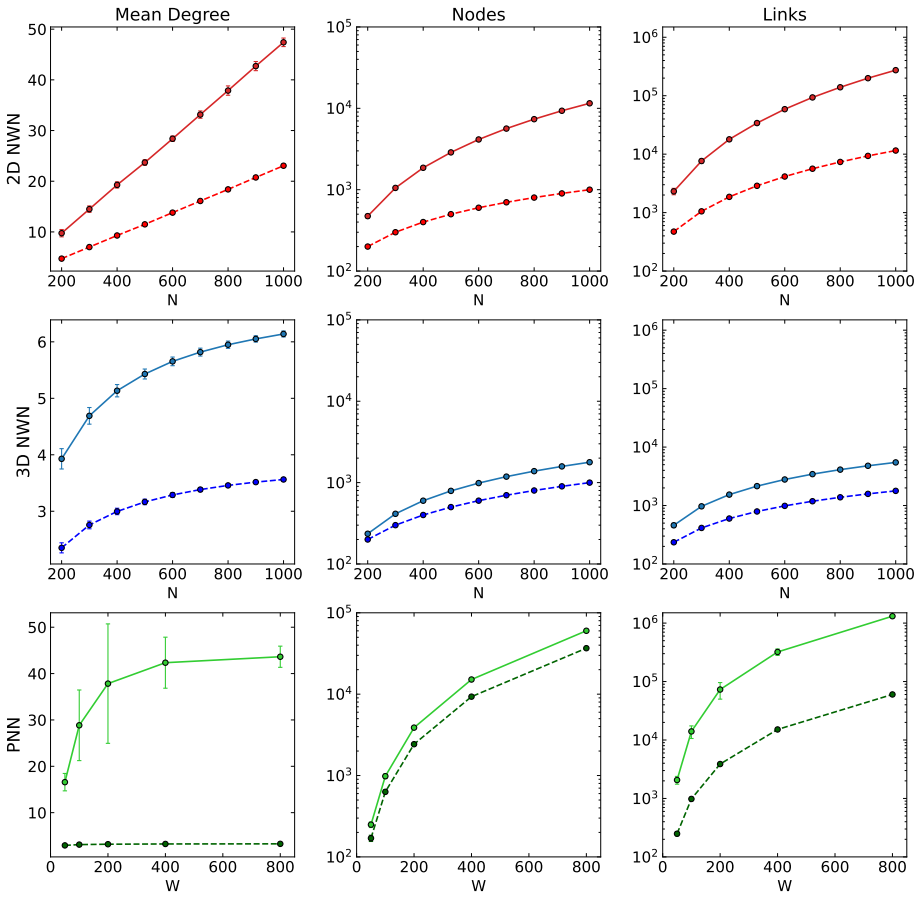

FIG. A1. Dependence of mean degree $\bar{k}$ (left column), the mean number of nodes (center), and mean number of links between nodes (right) on the number of nanowires, N (for the NWNs), and the system size, W (for the PNNs). 2D NWNs (top row, red), Q3D NWNs (middle row, blue) and PNNs (bottom row, green). SNMs: dashed lines; DNMs: solid lines. For the NWNs the transformation from the SNM to the DNM causes relatively modest changes in all three quantities. In contrast the transformation causes a dramatic increase in $\bar{k}$ for the PNNs, since the fractal groups of nanoparticles connect many tunnel gaps (see Figure 1 in the main text.)

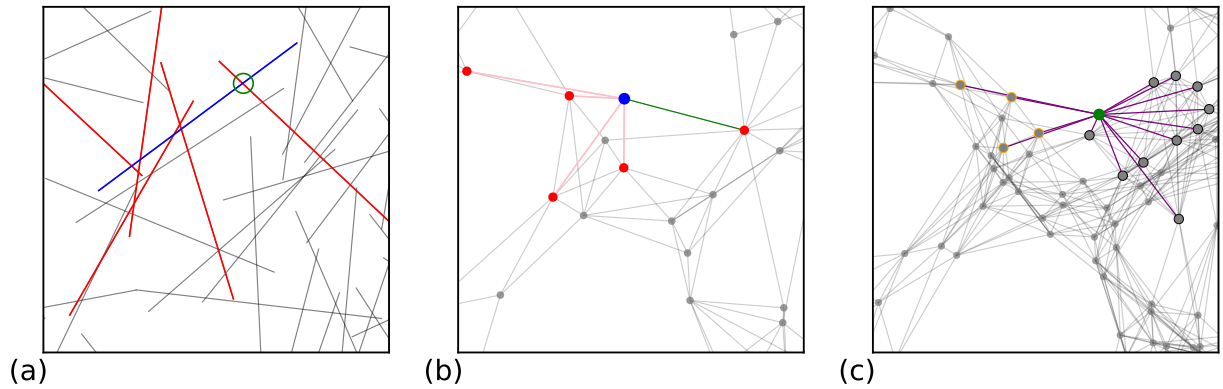

FIG. A2. (a) Portion of a nanowire network, highlighting a single wire (blue) and the wires it is connected to (red). (b) Static node map corresponding to (a). (c) Dynamic node map corresponding to (b).

APPENDIX B: ILLUSTRATION OF THE EFFECT OF THE TRANSFORMATION ON THE MEAN DEGREE.

The effect of the transformation from a static node map to a dynamic node map on the mean degree is described in this Appendix. Since the mean degree in the SNM is $\langle k \rangle$, which is greater than 1, the transformation to the DNM generates $\langle k \rangle$ times more nodes in the DNM. The number of links in the DNM is also significantly higher. This can be visualised for the specific example illustrated in Figure A2. The blue wire in (a) makes connections to 5 red wires (i.e. there are 5 memristive gaps), and so the degree of the blue node in the SNM shown in (b) is 5. Now consider the memristive gap highlighted by the green circle in (a) and represented by the green link in (b). This memristive gap is a node in the DNM (green node in (c)) and is connected to 4 other nodes (highlighted by the gold circles) *plus* the gaps between the far right red wire and any grey wire that crosses it (there are 10, highlighted by the black circles). Hence the degree of the green node in the DNM is significantly higher than that of the original blue wire in the SNM. The same is true for *every* memristive gap. The average degree of each node in the DNM is therefore higher than those in the SNM. And since the number of nodes in the DNM is already greater than that in the SNM, both N and $\langle k \rangle$ increase as a result of the transformation. These changes underpin the changes in other properties of the network that are discussed in the other figures.